Equilibrium Spatial Distribution of Aqueous Pullulan: Small-Angle X-ray Scattering and Realistic Computer Modeling

Jennifer H.-Y. Liu,[†] David A. Brant,*[,†] Shinichi Kitamura,[§] Kanji Kajiwara,[‡] and Mitsuru Mimura[‡]

Department of Chemistry, University of California, Irvine, California 92697-2025; Department of Biological Resource Chemistry, Kyoto Prefectural University, Shimogamo, Kyoto 606-8522, Japan; and Faculty of Engineering and Design, Kyoto Instituite of Technology, Kyoto 606, Japan

Received April 16, 1999; Revised Manuscript Received August 23, 1999

ABSTRACT: A rotational isomeric state model has been developed for the polysaccharide pullulan dissolved in water. The model is consistent with the mean-square radius of gyration and Debye scattering function as measured for pullulan oligomers containing 3, 6, 9, and 12 glucose residues by small-angle X-ray scattering. It is also consistent with the unperturbed chain dimensions of high molecular weight aqueous pullulan and the temperature coefficient of the unperturbed dimensions. The model is based on identification of an initial set of rotational isomeric states using the AMBER* molecular mechanics force field in conjunction with a continuum model for aqueous solvation. The relative weights of the rotational isomeric states were subsequently adjusted to achieve an optimized fit to the data. Three important rotational isomeric states (encompassing together more than 77% of the probability distribution) are identified for the (1→6)-linkage while a single state is recognized for the (1→4)-linkage. One of the states for the (1→6)-linkage may be stabilized by a hydrogen bond that spans the linkage and introduces a bend into the chain trajectory which serves to reduce the mean global dimensions of the chain.

Introduction

Pullulan is a linear glucan with the chemical structure {→6)-α-D-glucopyranosyl-(1→4)-α-D-glucopyranosyl-(1→4)-α-D-glucopyranosyl-(1→}$_n$.[1] A hexameric segment of pullulan containing a single central (1→6)-linkage is shown in Figure 1. Dimeric segments possessing a (1→4)- and (1→6)-glycosidic linkage are shown in Figure 2, a and b, respectively. Here the torsion angles ϕ_4 and ψ_4 of the (1→4)-linkage and ϕ_6, ψ_6, and ω_6 of the (1→6)-linkage are defined. Motions along these backbone torsional coordinates are the dominant source of pullulan chain tortuosity. Because the sugar rings are relatively rigid structural elements, it is often useful to think of the pullulan chain as a sequence of virtual bonds spanning the sugar residues to link the glycosidic oxygens of the chain backbone. These virtual bonds are not of fixed length, because the sugar rings are subject to flexing motions, and in the case of residues linked into the chain through C6′, the glycosidic O to glycosidic O distance is also dependent on the torsion angle ω_6. It is nevertheless beneficial to employ the virtual bond representation of the chain, and we will use this device frequently in what follows.

Because of its ready water solubility and its commercial availability in samples of narrow molecular weight distribution covering a wide range of mean molar masses, pullulan serves as a prototypical nonionic, water-soluble polysaccharide and as a calibration standard for aqueous size exclusion chromatography (SEC).[2−4] The measurable characteristics of aqueous pullulan have been investigated intensively with convincing agreement among the several studies.[5−12] Thus, the asymptotic characteristic ratio and persistence length

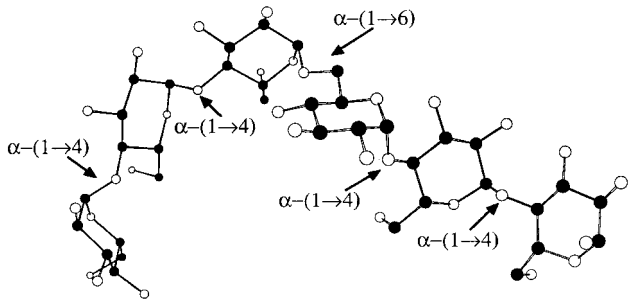

Figure 1. A hexameric segment of pullulan with a single (1→6)-linkage. Only carbon and oxygen atoms are shown.

and the chain length dependence of such aqueous solution properties as the intrinsic viscosity, the root-mean-square radius of gyration, the diffusion coefficient, the sedimentation coefficient, and the osmotic second virial coefficient can be extracted from the cited papers.

The equilibrium solution behavior of pullulan has been simulated at the atomistic level to produce satisfying agreement between the observed solution characteristics and the predictions of the model.[13−15] Both the absolute unperturbed polymer coil dimensions and the sign of the temperature coefficient of those dimensions are reproduced by the model, which describes a random coil chain with a weak tendency to follow a pseudo-helical trajectory.[15] The model suggests that directional correlations of the successive virtual bonds in the aqueous pullulan chain are lost completely over a range of approximately 15 residues. This correlation length, when expressed in units of contour length, is more commonly known as the Kuhn length in conventional polymer terminology.

Investigations of the conformational dynamics of aqueous pullulan and its oligomers in the nanosecond time domain have also been carried out using ^{13}C NMR relaxation as a probe of the local dynamics.[16] These studies reveal information about the rate of *temporal*

[†] Department of Chemistry.
[§] Department of Biological Resource Chemistry.
[‡] Faculty of Engineering and Design.
* To whom correspondence should be addressed.Telephone +1 (949) 824-6019; Fax +1 (949) 824-8571; e-mail dbrant@uci.edu.

10.1021/ma990591h CCC: $18.00
Published on Web 11/20/1999

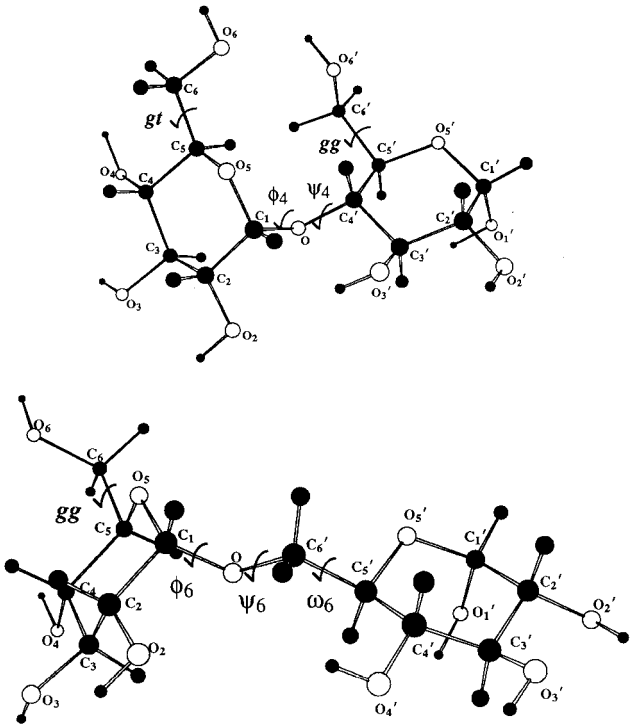

Figure 2. (a, top) A dimeric segment of pullulan illustrating the (1→4)-linkage. Glycosidic torsion angles $\phi_4(O_5-C_1-O-C_4')$ and $\psi_4(C_1-O-C_4'-C_5')$ are shown. (b, bottom) A dimeric segment of pullulan illustrating the (1→6)-linkage. Glycosidic torsion angles $\phi_6(O_5-C_1-O-C_6')$, $\psi_6(C_1-O-C_6'-C_5')$, and ω_6-$(O-C_6'-C_5'-O_5')$ are shown. The notation *gg* and *gt* refers to the rotational state of exocyclic torsion angle $\tau_6(O_5-C_5-C_6-O_6)$: $\tau_6(gg) \approx -60°$, $\tau_6(gt) \approx +60°$.

decay of directional correlations of the $^{13}C-^{1}H$ bond vectors associated with the resolvable ^{13}C nuclei in the polymer.[17−20] The molecular coordinates dominant in relaxations on this time scale are torsions about the chemical bonds of the chain backbone, predominantly the bonds of the glycosidic linkages between sugars and, to a lesser extent, the low-frequency vibrational modes of the sugar rings.[21,22] The observable NMR relaxation times, e.g., T_1 and T_2, are connected in an approximately inverse relationship to the *correlation times* τ associated with temporal relaxation of $^{13}C-^{1}H$ bond vector orientations.[19]

The relevant ^{13}C NMR relaxation studies disclose that the orientational relaxation behavior of the interior residues of pullulan oligomers match those of the interior residues of high molecular weight pullulan for oligomers of DP = 15 and greater.[16] Thus, the correlation length or wavelength of the segmental motions that cause the temporal decay of directional correlations of $^{13}C-^{1}H$ vectors in the interior of a pullulan chain is on the order of 15 residues, in good agreement with the decay length of spatial correlations described in the previous paragraph. A recent diffusive theory of polysaccharide dynamics indeed suggests a strong correlation between the correlation length for segmental motions and the Kuhn length of the chain.[23] Previous dynamics investigations also reveal that residues near the ends of oligomeric pullulans always display greater mobility (shorter correlation times) than interior residues regardless of DP. This means that not even the smallest oligomers behave as rigid bodies with respect to their nanosecond time scale dynamics.[16]

The present work is part of an ongoing effort to interpret the conformational dynamics of polysaccharides in terms of a structurally realistic models of the chain.[16,21,23,24] Rather than to explore the conformational dynamics of the polysaccharide chain in solution through (expensive) numerical simulations, we have adopted an analytic theory of polymer dynamics (optimized Rouse−Zimm (ORZ) theory), which is able to incorporate the realistic features of the chemical structure in any desired detail.[25−28] This approach employs equilibrium averaged structural characteristics, which may be obtained by numerical integration over the configuration space of the polymer expressed in the reduced coordinate space of the glycosidic torsional angles. Earlier conformational potential energy surfaces, refined to yield pullulan model behavior in accord with the characteristic ratio and its temperature coefficient for high molecular weight aqueous pullulan,[15] can be criticized on the grounds that they give heavy weight to fitting of the global conformational characteristics of the chain. In this work we report small-angle X-ray scattering (SAXS) studies of small pullulan oligomers in aqueous solution. SAXS data, particularly those from the upper accessible range of scattering angle, probe the shorter range features of the equilibrium spatial distribution of the chain.[29−31] The present SAXS data are used, in conjunction with the previous results for the global configurational properties of high molecular weight aqueous pullulan, to develop and refine conformational potential energy surfaces for the pullulan repeating units, which we intend to employ in theoretical models of the pullulan conformational dynamics.

Experimental Section

Sample Preparation. Pullulan oligomers were prepared by enzymic hydrolysis of high molecular weight pullulan (lot no. PM 250424, $M_n = 20.1 \times 10^4$, Hayashibara Biochemical Laboratories, Inc., Okayama, Japan) with *Klebsiella pneumoniae* pullulanase (lot no. P-5420 64H40561, Sigma Chemical Co., St. Louis, MO; suspension in 3.2 M $(NH_4)_2SO_4$, 100 units/2.2 mL). The enzyme is specific for the (1→6)-linkage in pullulan, so that the majority of the products of partial hydrolysis should be the oligomers $(G_3)_n$, where G_3 represents the (1→4)-linked repeating trimer maltotriose, and n is the number of trimeric repeating units in the oligomer. Here we will use the term degree of polymerization (DP) consistently to refer to the number n of repeating units in the oligomer $(G_3)_n$. Hydrolysis was carried out at 25 °C in pure water. The polymer was present at a concentration of approximately 100 mg/mL in a solution of 10 mL to which was added approximately 70 μL of the enzyme suspension. After 18−24 h, depending on the range of oligomers sought, the enzyme was deactivated by boiling for 60 min.

The hydrolysis product was filtered through a 0.45 μm Corning 25 mm cellulose acetate filter, and 3 mL of the filtered hydrolysate was applied to a 2 m × 22 mm stainless steel size exclusion chromatography (SEC) column packed with either Bio-Gel P4 or P6 (medium particle size, Bio-Rad Laboratories, Richmond, CA) depending on the oligomer size range in which maximum resolution was sought. The column was eluted at room temperature with degassed, pure water at a rate of approximately 25 mL/h. For some of the chromatographic runs the column was maintained at 55 °C. The column resolution was somewhat improved at the higher temperature, but a shorter column lifetime was experienced. In general, room temperature operation provided more satisfactory service from the column. Effluent was monitored with a differential refractometer (Waters model R401), and samples were collected in 5 mL aliquots with a fraction collector (LKB model 2111 Multirac). Corresponding fractions from successive SEC runs were pooled, stored at 4 °C, and subsequently freeze-dried to recover the solid oligomeric products.

A typical SEC chromatogram from Bio-Gel P4 is shown in Figure 3a. Peaks 1, 2, 3, etc., were presumed initially to consist

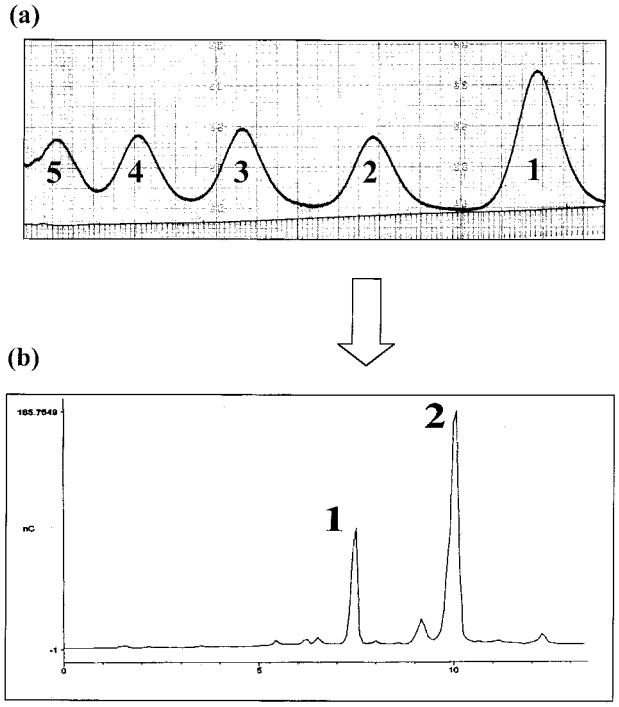

Figure 3. (a) SEC chromatogram of pullulan oligomers G_3-$(G_3)_5$ and (b) HPAEC chromatogram of pullulan oligomer $(G_3)_2$. The concentration of $(G_3)_2$ for HPAEC was 0.1 mg/mL.

Table 1. Composition of SAXS Samples[a]

nominal DP →	1	2	3	4
W_1	1	0.238	0.230	0.141
W_2		0.762	0.160	0.070
W_3			0.610	0.149
W_4				0.640
Z_1	1	0.137	0.095	0.044
Z_2		0.863	0.135	0.041
Z_3			0.770	0.136
Z_4				0.779

[a] W_i = weight fraction of oligomer with DP = i. Z_i = z-fraction of oligomer with DP = i.

primarily of the oligomers G_3, $(G_3)_2$, $(G_3)_3$, etc., respectively. Subsequent analysis of these peaks with high-performance anion exchange chromatography (HPAEC) using a Dionex DX 500 system revealed that they did not consist of the pure oligomers. HPAEC peaks were assigned and calibrated using authentic samples of the several oligomers. Detector response is very nearly directly proportional to the concentration of hydroxyl groups contributed by a given compound and, hence, to the mass of oligomer contained in the detector cell.[32] The actual compositions of samples used for the SAXS investigations, expressed as the directly measurable weight fraction W_n of the oligomer $(G_3)_n$, are shown in Table 1. Each SAXS sample is identified in the table by its nominal DP (1 through 4). A typical HPAEC chromatogram for the sample of nominal DP = 2 is shown in Figure 3b. Negligible amounts of species other than G_3, $(G_3)_2$, $(G_3)_3$, and $(G_3)_4$ were detected in the samples submitted to SAXS analysis.

The proportions of the various oligomers in the SAXS samples are also expressed as z-fractions in Table 1 for subsequent use in the refinement procedure, since experimental SAXS data on polydisperse systems (Debye scattering function and mean-square radius of gyration) are z-averages over the mass distribution.[33] The z-average of any property A is defined by

$$\langle A \rangle_z = \sum_n Z_n A_n \tag{1}$$

and Z_n is related to W_n by

$$Z_n = W_n M_n / \sum_i W_i M_i \tag{2}$$

where M_i is the molar mass of oligomer with DP = i.

SAXS Methodology. Small-angle X-ray scattering experiments were conducted at the Photon Factory, Tsukuba, Japan, using the SAXES (small-angle X-ray scattering equipment for solutions) spectrometer using the following procedures.[34] Oligomers with DP = 1, 2, 3, and 4 were dissolved in pure water at a concentration of 25 mg/mL, and the experiments were conducted at 25 °C. Samples were contained in flat cells (1 cm × 0.5 cm × 0.2 cm) fitted with a pair of thin mica windows. Incident X-rays from synchrotron radiation were monochromatized to λ = 1.488 Å with a double-crystal monochromator and then focused at the cell position with a bent focusing mirror. The scattered X-rays were detected using a one-dimensional position-sensitive proportional counter (PSPC) with effective length 160 mm positioned 1−2 m from the sample holder. The scattered intensity from each sample was corrected for variation of the incident X-ray flux by monitoring the beam with an ionizing chamber placed in front of the thermostated sample holder. The excess scattering intensity was obtained by subtracting the scattering intensity of water from those of the solutions. The SAXS intensities were accumulated for a measuring time of 15−30 min, sufficient to attain a satisfactory signal-to-noise ratio. Data were collected on a CAMAC data acquisition system controlled by a NEC PC 9801RX. The scattering intensity $P(q)$, normalized by the intensity at scattering angle θ = 0, was observed over the range of the scattering vector $q = (4\pi/\lambda)\sin(\theta/2)$ from 0.025 to 0.500 Å^{-1}, which means that the Bragg spacings in the range 13−250 Å were explored.

Unrefined Conformational Energy Surfaces

Conformational energy surfaces were calculated for the disaccharides shown in Figure 2a,b using a commercial molecular mechanics software package (MacroModel 5.5, Columbia University).[35] Energies are expressed in what follows as a function of the glycosidic torsion angles ϕ_4 and ψ_4 for the (1→4)-linked disaccharide in Figure 2a and as a function of ϕ_6, ψ_6, and ω_6 for the (1→6)-linked disaccharide in Figure 2b. Energies were calculated on a regular grid with spacing of 20° in $\phi,\psi,(\omega)$ space by imposing an artificially large torsional energy barrier on the torsion angles in question. At each grid point the remaining coordinates of the disaccharide configuration space were allowed to relax using the BatchMin (ENRGY/MINIM/PRCG) energy minimizer supplied in the software package. Cutoffs were set at 10 and 20 Å for van der Waals and electrostatic interactions, respectively. The AMBER* force field (adjusted to the specific requirements imposed by application to carbohydrates) as supplied in the software package was used, and the effects of aqueous solvation were estimated by using the GB/SA continuum solvent model for water.[36,37]

We were not particularly concerned with the extent to which the minimizer in the software package succeeds in finding the absolute minimum at each grid position: It was our intention from the outset to adjust any initial approximation to the pullulan conformational potential surface in order to achieve the best possible agreement of computed characteristics of pullulan with the SAXS data reported here on pullulan oligomers and earlier results for the global dimensions of high molecular weight aqueous amylose. Projection of the relaxed conformational energy onto torsion angle space is consistent with the philosophy of the ORZ polymer dynamics treatment in which coordinate space is reduced to those slow coordinates most significant for the diffusive motions of the chain.[25−28]

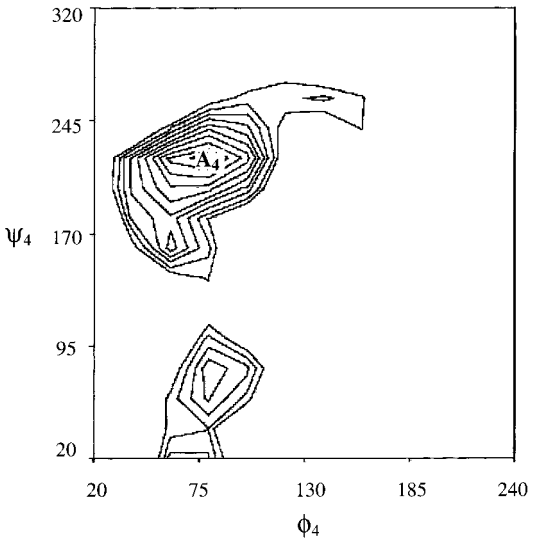

Figure 4. Potential energy surface for the (1→4)-linked disaccharide of Figure 2a. The contour interval is 0.5 kcal/mol relative to the minimum-energy conformation at A_4. The details are described in the text.

The conformational energy surfaces calculated as described above for the (1→4)- and (1→6)-linked disaccharides are shown in Figures 4 and 5, respectively. The contour interval is 0.5 kcal/mol relative to the energy minimum on each surface. Significant minima are labeled A_4, A_6, B_6, C_6, etc. For the (1→4)-linkage only the principal minimum A_4 makes significant contributions to the properties of the system; for the (1→6)-linkage there are potentially six important linkage conformations. Note that parts a and b of Figure 5 are sections through the three-dimensional contour map taken at $\phi_6 = 80°$. Most of these minima are deepest for $\phi_6 = 80°$, and the energy rises steeply, and approximately symmetrically, as ϕ_6 deviates from this preferred state. Hence, we have chosen $\phi_6 = 80°$ to display the allowed conformations of the torsion angle ϕ_6.

Parts a and b of Figure 5 correspond to two different assumptions about the preferred rotational state of the exocyclic torsion angle $\tau_6(O_5-C_5-C_6-O_6)$. This torsion angle is shown in Figure 2b in the *gg* rotational state; Figure 2a shows both the *gg* and *gt* states. Of the three staggered rotational states of this bond ($gg \approx -60°$, $gt \approx +60°$, and $tg \approx \pm 180°$), experimental evidence shows that only *gg* and *gt* are energetically accessible.[38−40] In what follows we consequently ignore the *tg* state in which O_5 and O_6 are in the trans relationship. A naive consideration of the system might suggest that the trans state would be favored, but it is well-known to be disfavored by the stereoelectronic *gauche effect*.[41−43] The gauche effect, and the similar anomeric and exoanomeric effects, require special handling in the parametrization of molecular mechanics force fields, such as AMBER*, intended for use with carbohydrates.[44−46]

It may be seen from Figure 5a,b that the relative energies of the several minima on the (1→6) surface, and the relative frequency of occupancy, are affected by the *fixed* choice of τ_6. In particular, the relative importance of minimum C_6 is different in the two maps. We note that minimum C_6 is not as pronounced when some other molecular mechanics force fields are used, and it may be stabilized in part by effects peculiar to the force field and solvation treatment adopted here. It can, of course, be argued that the appropriate energy surface

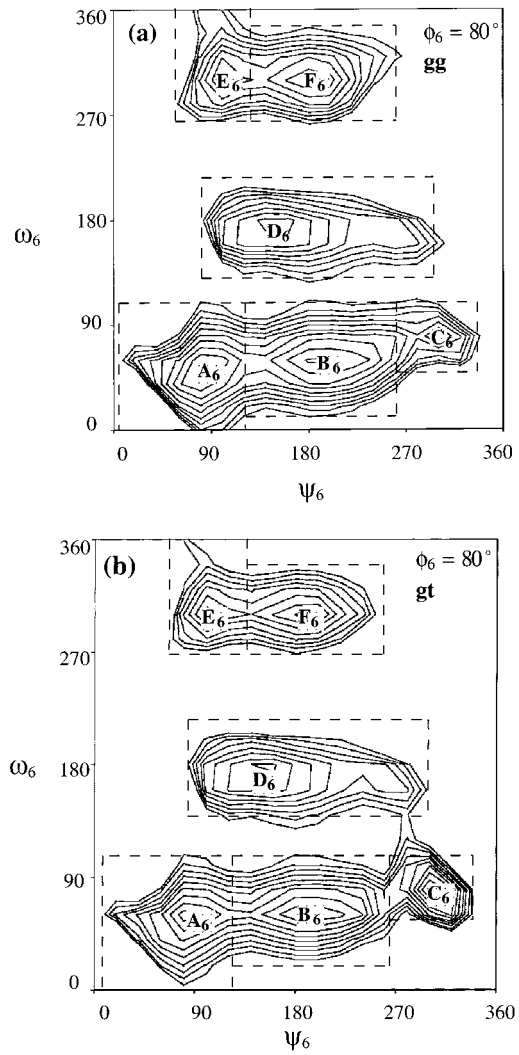

Figure 5. Potential energy surface for the (1→6)-linked disaccharide of Figure 2b. Glycosidic torsion angle ϕ_6 is fixed at 80°. (a) Exocyclic torsion angle τ_6 is fixed at −60° (*gg*). The contour interval is 0.5 kcal/mol relative to the minimum-energy conformation at B_6. (b) Exocyclic torsion angle τ_6 is fixed at +60° (*gt*). The contour interval is 0.5 kcal/mol relative to the minimum-energy conformation at C_6.

for the (1→6) surface is, in the present context, that averaged over the states of τ_6. A surface minimized with inclusion of τ_6 among those variables allowed to relax always corresponds to predominance of the *gt* state, in clear contradiction to abundant experimental evidence.[38−40] We choose instead to recognize in the refinement process described below that the chain properties must reflect some mixing of the *gg* and *gt* states of τ_6, and we have, in effect, used the mixing proportions as one of the refinement parameters. Clearly, the torsional states of τ_6 and $\tau_{6'}$ will also affect the details of the conformational energy map for the (1→4)-linkage (Figure 4). For no combination of the possible allowed staggered states of τ_6 and $\tau_{6'}$, however, is minimum A_4 supplanted as the dominant minimum. Hence, in the present context, there is no need to consider several maps for the (1→4)-linkage.

If it is assumed that the conformational energy of the entire polysaccharide chain can be approximated as a sum of independent contributions, one associated with each glycosidic linkage of the backbone, then the conformational energy of the chain in any particular conformation can be determined from the conforma-

tional energy surfaces of the representative dimeric segments in Figures 4 and 5. We adopt this approach, which has long precedent.[47−49] Independence of successive glycosidic linkages is tantamount to ignoring the excluded-volume effect, because only the interactions of sequentially adjacent residues are included.[49] The excluded-volume effect is negligible in the short pullulan oligomers considered here,[30,50] and in making comparisons of computed chain properties with the experimental properties of high molecular weight pullulan, we confine attention exclusively to measured properties[8] referred to the unperturbed state of the polymer coil.[51]

Computation of Mean Chain Characteristics

Statistical Weights. Computation of measurable characteristics of pullulan, e.g., unperturbed mean-square radius of gyration, $\langle s^2\rangle_0$, Debye scattering function, $P(q)$, requires averaging over the conformation space of the polymer chain. We elect to do this using the conventional rotational isomeric state (RIS) approach with the several minima of Figures 4 and 5 chosen as the isomeric states.[52,53] Statistical weights σ_i for each state $i = A_6, B_6, C_6$, etc., are assigned as the fraction, attributable to state i, of the configuration integral over ϕ,ψ,ω space for the (1→6)-linkage. The configuration integral is approximated by summation on the same 20° grid in torsion angle space that was used to compute the conformational energy surface. The somewhat arbitrary subdivision of the conformation space for the (1→6)-linkage is shown by the rectilinear dashed lines in Figure 5a,b; the bounds in the ϕ dimension were taken for all minima to be $20° \le \phi \le 120°$. Thus, σ_i is given by

$$\sigma_i = \frac{\sum_i \exp\{-E(\phi,\psi,\omega)/RT\}}{\sum_{\text{all}} \exp\{-E(\phi,\psi,\omega)/RT\}} \tag{3}$$

where $E(\phi,\psi,\omega)$ represents the molar conformational energy of the disaccharide, the summation in the denominator covers the range $0 \le \phi,\psi,\omega \le 2\pi$, and the summation in the numerator is limited to the range of ϕ,ψ,ω associated with RIS i. Because only one RIS has been identified on the conformational energy surface for the (1→4)-linkage, its statistical weight is necessarily unity. It would be inappropriate to choose only a single RIS for the (1→4)-linkage, if it were our purpose to treat the properties of the (1→4)-linked α-D-glucan homopolymer. It is, however, acceptable in the present instance where the majority of the flexibility of the pullulan chain derives from the (1→6)-linkage. (Flexibility in this context refers to the accessibility of torsion angle space and increases with an increase in the accessible fraction of the torsion angle space associated with a given linkage type.[47])

The position $\langle\phi_i\rangle,\langle\psi_i\rangle,\langle\omega_i\rangle$ in the torsion angle space of RIS i was assigned at the mean values of the angles $\theta_i = \phi_i$, ψ_i, and ω_i as computed from

$$\langle\theta_i\rangle = \frac{\sum_i \theta_i \exp\{-E(\phi,\psi,\omega)/RT\}}{\sum_i \exp\{-E(\phi,\psi,\omega)/RT\}} \tag{4}$$

Table 2. Locations and Statistical Weights of RIS for the (1→4)- and (1→6)-Linkages

RIS	RIS location $\langle\phi_i\rangle,\langle\psi_i\rangle,\langle\omega_i\rangle$	initial statistical weight σ_i (model 3)	refined statistical weight σ_i (model 4)
A_4	75,218	1.00	1.00
A_6	69,80,54	0.307	0.264
B_6	71,190,62	0.447	0.352
C_6	84,300,80	0.035	0.158
D_6	74,156,174	0.112	0.076
E_6	76,105,301	0.024	0.055
F_6	74,179,301	0.075	0.095

where both summations are restricted to the domain of RIS i. The location for RIS A_4 was determined in a similar way. The locations and initial statistical weights for RIS states A_4, A_6, B_6, C_6, etc., are given in Table 2. For the (1→6)-linkage the initial statistical weights and RIS locations are 50/50 weighted averages from Figure 5a,b, as suggested by the experimentally observed distribution of τ_6 states.[40]

Calculated Properties. The primary SAXS observable is the normalized Debye scattering function $P(q) = I(q)/I(0)$, where $I(q)$ is the absolute intensity of scattered radiation corresponding to scattering vector $q = (4\pi/\lambda)\sin(\theta/2)$ and $I(0)$ is the scattering intensity extrapolated to $q = \theta = 0$. For any set of atomic scattering centers $P(q)$ may be expressed in terms of the interatomic distances r_{ij} by the Debye formula.[54]

$$P(q) = \sum_{i=1}^{n} g_i^2 \phi_i^2(q) + 2\sum_{i=1}^{n-1}\sum_{j=i+1}^{n} g_i g_j \phi_i(q)\,\phi_j(q)\left\langle \frac{\sin(r_{ij}q)}{r_{ij}q}\right\rangle \tag{5}$$

For molecules in solution, computation of $P(q)$ from an atomistic model requires ensemble or time averaging over the host of configurations that the molecule can adopt, and this average is implied by the angle brackets in eq 5. We describe below a Monte Carlo approach to obtaining the ensemble average. In all that follows the symbol $P(q)$ will be understood as the ensemble averaged quantity required for comparison with experiment.

In the Debye formula g_i is the net scattering power of atom i, conventionally taken as the atomic number, i.e., number of electrons, of atom i less the mean atomic number of the background solvent. For water the mean atomic number is 0.336 electrons/Å^3 × V_i Å^3, where V_i is the volume of atom i computed on the assumption that atom i is a sphere of radius R_i. The quantity $\phi_i(q)$ is the atomic form factor for atom i, usually approximated by

$$\phi_i(q) = \frac{3[\sin(R_i q) - (R_i q)\cos(R_i q)]}{(R_i q)^3} \tag{6}$$

This expression for $\phi_i(q)$ assumes uniform electron density within a sphere of radius R_i, often approximated as the van der Waals radius, R_{iv}, of the atom. More accurate versions of $\phi_i(q)$ can be obtained from tabulations based on quantum mechanical calculations of atomic electron distribution.[55] We find that the accurate tabulated form factors for carbon and oxygen can be approximated very closely by substituting $R_i = 0.6R_{iv}$ in eq 6. Table 3 gives values of $\phi_i(q)$ from the tablulations, from eq 6 with $R_i = R_{iv}$, and from eq 6 with $R_i = 0.6R_{iv}$ for several values of q in the experimentally relevant range.

Table 3. Atomic Form Factors

q, Å^{-1}	C[a]	C[b]	C[c]	O[a]	O[b]	O[c]
0.0	1.0	1.0	1.0	1.0	1.0	1.0
0.1257	0.9983	0.996	0.998	0.9990	0.996	0.999
0.2513	0.9930	0.982	0.994	0.9959	0.986	0.995
0.3770	0.9845	0.961	0.986	0.9908	0.968	0.989
0.5027	0.9728	0.931	0.975	0.9836	0.944	0.980

[a] Tabulated values.[55] [b] Equation 6 with $R_i = R_{iv}$. [c] Equation 6 with $R_i = 0.6R_{iv}$.

Only carbon and oxygen atoms are included in the sum in eq 5; the contribution of hydrogen atoms to the X-ray scattering is ignored. Note that whenever we equated R_i to R_{iv} in eq 6, we also computed the mean atomic number of water using $R_i = R_{iv}$. Likewise, whenever we used $R_i = 0.6R_{iv}$ in eq 6, we used $R_i = 0.6R_{iv}$ to compute the mean atomic number of water. The rationale for using $0.6R_{iv}$ to compute the volume of water displaced by a given atom is that the atoms displacing water are all bonded, and the van der Waals radius overestimates their effective radii. Clearly the choice $R_i = 0.6R_{iv}$ is one approximation among several that could have been adopted. It means that both factors in the products $g_i\phi_i$ occurring in eq 5 are increased when we take $R_i = 0.6R_{iv}$ instead of $R_i = R_{iv}$.

The approach of $P(q)$ to $P(0)$ contains information about the overall size of the subject molecule expressed in terms of the mean-square radius of gyration $\langle s^2\rangle_0$; the subscript 0 recognizes explicitly the short-range character of the potential energy surface employed here. The quantity $\langle s^2\rangle_0$ is calculable directly from the atomic coordinates of any molecule in a Monte Carlo sample using the definition[52]

$$\langle s^2\rangle_0 = \sum_1^k m_i s_i^2 / \sum_1^k m_i \tag{7}$$

Here s_i is the distance of atom i from the center of mass of a collection of k atoms, m_i is the mass of atom i, and the angle brackets imply the statistical mechanical average over all configurations that the collection of atoms can adopt. Alternatively, one can compute $\langle s^2\rangle_0$ from the interatomic distances r_{ij} using the theorem of Lagrange.[52] Experimentally, $\langle s^2\rangle_0$ is extracted from the dependence of $P(q)$ on q using the Guinier approximation[56]

$$P(q) \cong \exp(-\langle s^2\rangle_0 q^2/3) \tag{8}$$

applicable to the limiting behavior of of $P(q)$ at low angle.

Monte Carlo Averaging. To compute $P(q)$ and $\langle s^2\rangle_0$ using eqs 5 and 7, we generate a sample of oligomeric or polymeric pullulan chains of the desired DP in fixed conformations consistent with the potential energy surfaces for the glycosidic linkages approximated by Figures 4 and 5. Using a rigid *mean* sugar residue geometry representative of those that correspond to the minima on these conformational energy surfaces, pullulan chains are constructed with glycosidic linkage torsion angles ϕ,ψ,ω that are assigned values using a simple Monte Carlo procedure. Statistical selection of torsion angles is required only for the (1→6)-linkages, because just one RIS is permitted to the (1→4)-linkages in the present treatment. Thus, we define the cumulative distribution function $F(j)$ by

$$F(j) = \sum_i^j \sigma_i \tag{9}$$

for $i = A_6$, B_6, C_6, etc., for the several RIS states of the (1→6)-linkage. This is a multistep function with, in this case, six steps of varying height and with $F(6) = 1$. The height of each step is equal to the probability of occupancy of the corresponding RIS for the (1→6)-linkage. Hence, random numbers in the interval 0−1 can be used to select a sequence of RIS states for the independent (1→6)-linkages of pullulan with a frequency distribution dictated by the conformational energy surfaces in Figure 5 and given in Table 2. The mean values of $\sin(r_{ij}q)/r_{ij}q$ averaged over all chain conformations and needed in eq 5 are computed as simple arithmetic means from the Monte Carlo sample for each interatomic distance r_{ij} and each relevant value of the angular variable q. In our experience a sample of 5000 chains suffices to achieve well-converged mean values. Actual generation of the polymer chains in the Monte Carlo sample was carried out with software written specifically for this purpose. Details are provided elsewhere.[30,50,57]

The procedure just described is carried out for a polymer or oligomer of a given DP. For comparison with experimental results on the paucidisperse samples actually subjected to SAXS investigation, the computed results for $P(q)$ and $\langle s^2\rangle_0$ were averaged with z-fraction weighting as described in eq 1.

Results and Discussion

The experimental SAXS data are shown for pullulan oligomers with DP = 1, 2, 3, and 4 as open circles in Figures 6−9, respectively. Data are plotted as $q^2P(q)$ against q after Kratky[54] in a form that is often able to highlight structural differences among samples.[58] The model-independent global size parameter $\langle s^2\rangle_0$ is determined by the low-angle behavior of $P(q)$; the shorter range structural features contribute increasingly to determining the value of $P(q)$ as q increases. We observe that the high-angle experimental data are somewhat less certain that those at low angle, not only because of weaker scattering intensity and, hence, poorer signal-to-noise ratio but also because larger instrumental corrections must be applied to the off-axis data. The experimental root-mean-square radii of gyration $R_g = \langle s^2\rangle_0^{1/2}$, determined by fitting the low-q data with eq 8, are given as insets in Figures 6−9. Observed experimental uncertainties in all measured R_g values are about ±2.5%.

Several curves are drawn on each of Figures 6−9. These correspond to various stages of refinement of the theoretical model. The curve for model 1 shows the scattering function $q^2P(q)$ calculated using the initial statistical weights in Table 2, taking $R_i = R_{iv}$, and without correcting the calculated $P(q)$ values for the paucidispersity of the oligomers with DP = 2, 3, and 4. The values of R_{iv} used were 1.67 and 1.50 Å for C and O, respectively. The corresponding value of R_g calculated using eq 7 is indicated in Figures 6−9. Model 1 appears to fit the low-q data for $q^2P(q)$ and reproduces the experimental R_g values reasonably well, although the quality of the fit to R_g diminishes as DP increases. The fit to the high-q data is poor. When the paucidispersity of samples with DP = 2, 3, and 4 is taken into account

(model 2), all of the calculated curves move up slightly. The fits to the experimental R_g values are improved marginally, but the fit to $q^2P(q)$ at high q is not materially improved. The modest effect of the paucidispersity correction reflects the dominance of the heaviest, and most abundant, component of the distribution in determining the z-average (Table 1).

Using eq 6 with $R_i = R_{iv}$ implies uniform atomic electron density within a sphere of radius R_{iv}. This is clearly at odds with the electron density profile of real atoms. This approximation can be greatly improved simply by using eq 6 with $R_i = 0.6R_{iv}$ (Table 3). Model 3 implements this simple correction, and a greatly improved fit to the high q data is achieved. The improvement at high q reflects the contributions from short-range interference effects to $P(q)$; the data at small q depend entirely upon longer range interference effects that are not affected by the detailed scattering behavior of the individual atoms but only on their relative spatial positions. Consequently, there is no change in the calculated values of R_g in progressing from model 2 to model 3.

The final stage of refinement (model 4) involves making modest adjustments of the relative statistical weights of the several RIS states for the (1→6)-linkage to achieve optimal fit to the experimental data in Figures 6−9. The refined statistical weights are presented in column 4 of Table 2. The marked improvements in the fits to R_g and the scattering curve (Kratky plot) at high q effected by model 4 result from simple reassignment of the relative importance accorded the conformational energy surfaces for the (1→6)-linkage presented in Figure 5a,b. The initial statistical weights in Table 2 assumed equal contributions from the surfaces corresponding to the *gg* and *gt* states of torsion angle τ_6. Model 4 weights the states 40% (*gg*) and 60% (*gt*); the relative weights remain within the experimentally observed range.[40] Note that RIS C_6 assumes a more prominent role in model 4, predominantly at the expense of states A_6, B_6, and D_6.

At this stage we also take into account earlier data on R_g for high molecular weight aqueous pullulan and the experimental temperature coefficient of this parameter. For convenience in displaying simultaneously the high and low molecular weight data, we focus on the parameter $\langle s^2\rangle_0/N$, where $N = 3\text{DP}$ is simply the number of glucose residues in the polymer or oligomer chain. In the limit of very large chain length this parameter approaches a constant value known for aqueous pullulan to be 15.0 ± 0.7 Å^2 at 25 °C; the experimental temperature coefficient $\mathrm{d}\ln(\langle s^2\rangle_0/\mathrm{N})/\mathrm{d}T$ is -0.0043 K^{-1}.[8] The uncertainty (experimental and systematic) in the temperature coefficient is approximately equal to its magnitude; only the sign can be considered reasonably reliable.

The fit to $\langle s^2\rangle_0/N$ achieved with model 4 over the entire range of chain length is shown in Figure 10, where the experimental results are displayed as triangles (with error bars) and the results from model 4 are shown as circles. Not only are the experimental R_g values and Kratky plots for the oligomers reproduced very well, but model 4 also matches the experimental value of $\langle s^2\rangle_0/N$ for the high polymer within the uncertainty of that result. The theory yields a negative value for $\mathrm{d}\ln(\langle s^2\rangle_0/N)/\mathrm{d}T$, but one considerably smaller in magnitude than that measured experimentally. Because $\mathrm{d}\ln(\langle s^2\rangle_0/N)/\mathrm{d}T$ is exceptionally difficult to determine accurately from solution measurements,[52] we are satisfied to have reproduced the sign of this parameter with the theory. It will be noted from Figures 6−9 that, except for the oligomer with DP = 1, moving from model 3 to model 4 results in smaller, and more accurate, calculated values of R_g. The same trend is observed for the high polymer. Models 1−3 produce values of R_g for the high polymer that are approximately 15% too large. Thus, attribution of greater weight to RIS C_6 in model 4 coincides with a decrease in the computed polymer chain dimensions.

Calculations of $\langle s^2\rangle_0/N$ for comparison with the high molecular weight results were not carried out using eqs 5−7 with Monte Carlo sampling, because the slow

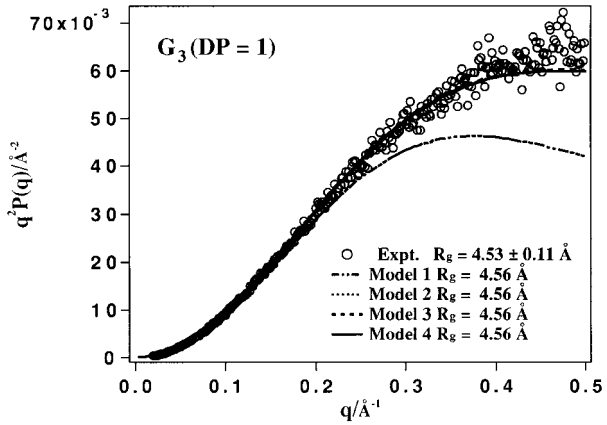

Figure 6. Kratky plot ($q^2P(q)$ vs q) for pullulan oligomer G_3 (DP = 1).

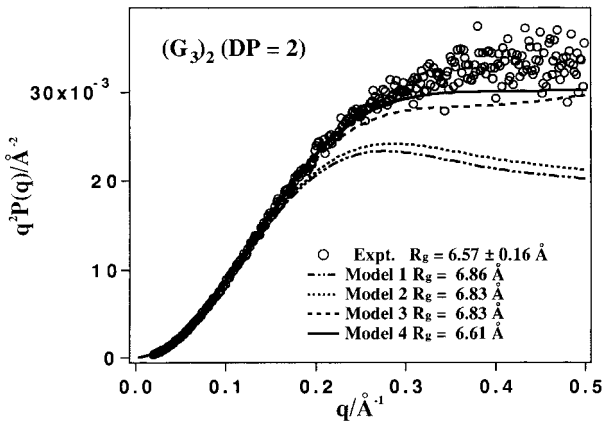

Figure 7. Kratky plot ($q^2P(q)$ vs q) for pullulan oligomer $(G_3)_2$ (DP = 2).

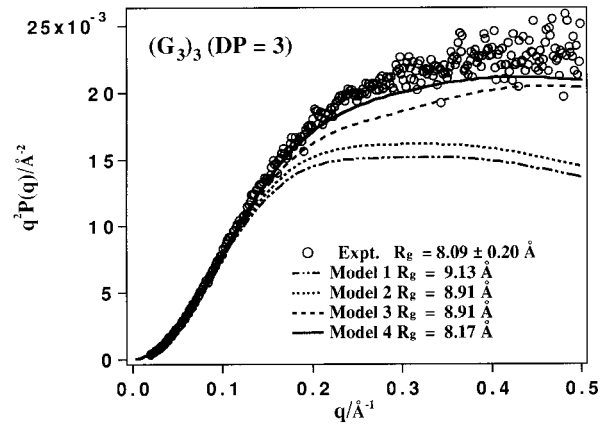

Figure 8. Kratky plot ($q^2P(q)$ vs q) for pullulan oligomer $(G_3)_3$ (DP = 3).

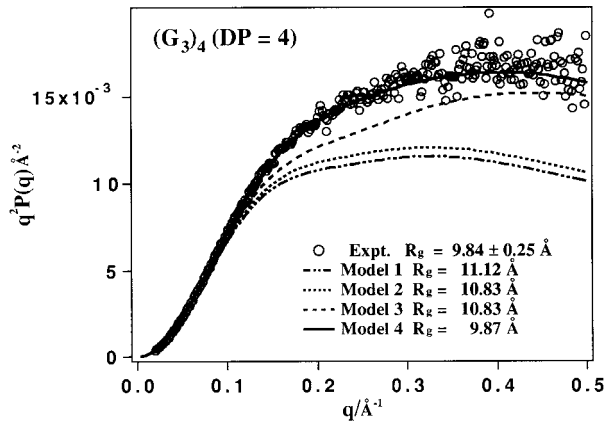

Figure 9. Kratky plot ($q^2P(q)$ vs q) for pullulan oligomer $(G_3)_4$ (DP = 4).

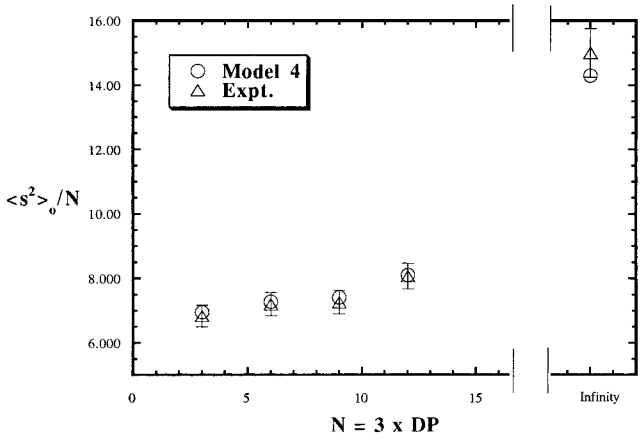

Figure 10. Comparison of experimental (△) and calculated (○) values of $\langle s^2\rangle_0/N$ for pullulan oligomers and high molecular weight pullulan. Error bars display estimated error in the experimental data.

convergence of $\langle s^2\rangle_0/N$ to its asymptotic limit made this approach computationally inconvenient. Furthermore, $d\ \ln(\langle s^2\rangle_0/N)/dT$ was difficult to determine due to the statistical error from Monte Carlo sampling. Instead, we used well-established methods[52,53] that permit rapid access to the asymptotic result. Specific details of application of these "G-matrix" methods to pullulan have been given earlier.[15] It is conventional with polysaccharides to consider only the glycosidic oxygens rather than the full assemblage of atoms in each sugar residue when computing $\lim_{N\to\infty}\langle s^2\rangle_0/N$ in this way. This entails no approximation, since in this limit only the spatial separations of chain segments remote from one another in the chain sequence contribute to $P(q)$.

The excellent fit achieved with model 4, which gives significant weight to RIS C_6, appears to confirm the importance of this conformation intially suggested by the AMBER* force field in conjunction with the GB/SA continuum solvent model. It became clear during the refinement procedure that larger proportions of state C_6 were associated with more compact chain configurations for all but the smallest oligomers. Examination of molecular models suggests that RIS C_6 may be stabilized in part by a hydrogen bond between O6 and O1′ (the succeeding glycosidic oxygen) when τ_6 is in the *gt* state, as shown in Figure 11. This interaction across the (1→6)-linkage, which contributes significantly to the importance imputed to the C_6 state by AMBER* plus GB/SA solvation in Figure 5b, serves to introduce a bend

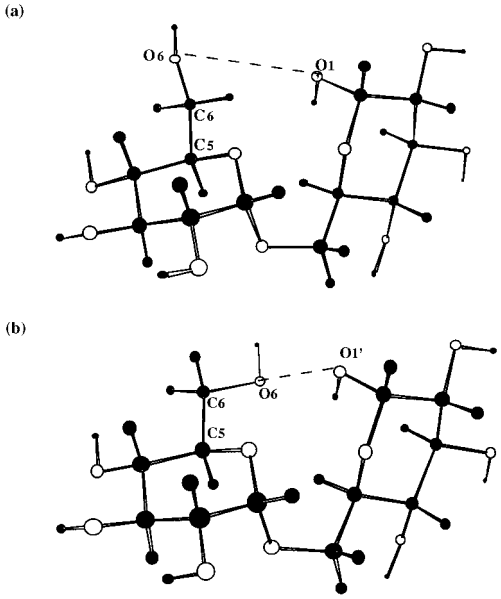

Figure 11. Drawing of the (1→6)-linked disaccharide (Figure 2b) in the C_6 conformational state with (a) *gg* and (b) *gt* conformer of C_5-C_6 torsion angle τ_6. The distance (dashed line) between O_6 and O_1' is (a) about 4 Å and (b) 2.5−3 Å.

into the chain and hence to diminish the mean chain extension relative to models which give less weight to this RIS.

Glycosidic oxygens are not ususally effective hydrogen bond receptors, and it should be recognized that this interaction is suggested by molecular mechanics calculations carried out for a disaccharide unit in which this oxygen was in hydroxylic rather than glycosidic form. It is noteworthy, however, that the crystal structure of panose {*O*-α-D-glucopyranosyl-(1→6)-*O*-α-D-glucopyranosyl-(1→4)-D-glucose}, a trisaccharide fragment from the pullulan chain, does display several instances in which glycosidic oxygens serve as receptors for bifurcated hydrogen bonds.[59] Panose is of further interest for the occurrence of an exocyclic torsion angle $\tau_6(O_5-C_5-C_6-O_6)$ in approximately the *tg* ($\approx\pm180°$) state. Occurrence in panose of this rare conformation of τ_6 is clearly a consequence of crystal packing factors and does not vitiate exclusion of this torsional state in the present work. It is worth remarking finally that when the (1→6)-linkage in pullulan adopts the conformation C_6, some unacceptably short contacts are initiated between second neighboring glucose residues in the panose fragment. These can be relieved by small adjustments of the intervening glycosidic torsion angles in keeping with the spirit of the RIS approach, in which each RIS state represents a family of similar conformers. Explicit consideration of second-neighbor interactions is outside the scope of the independent residue approximation used here. Such features of the true potential energy surface are, in effect, subsumed into the potential of mean force, when the statistical weights of the several RIS states are adjusted to achieve the best fit to experimental data.

Other workers have used molecular mechanics to investigate the characteristics of the (1→6)-linked dimeric segment of pullulan (isomaltose) shown in Figure 2b. Dowd et al. identify seven minima on the surface using the MM3(92) force field with no explict accounting for the effects of solvation.[60] These minima are readily identified with the minima in Figure 5a,b. The seventh

and most energetic of the MM3(92) minima corresponds to the high, shallow minimum located near $\psi_6 = 270°$ in RIS D_6. We did not consider this a separate RIS, because of its relatively high energy as calculated using AMBER* with the GB/SA solvation treatment. The minimum is also too high in energy on the MM3 surface to be of any practical importance. Tvaroska et al., using a continuum model to approximate the effects of solvation, report the six mimima found here and by Dowd et al. plus four additional minima that cannot be identified with states A_6 through F_6.[61] These four additional states occur with values of ϕ_6 in the range 140−160°, well beyond the accessible range of ϕ_6 determined here and by Dowd et al. and outside the range normally considered to be allowed for ϕ_6 by the exoanomeric effect.[43,62,63] Recent computations using the Cerius^2 software package[64] with implementation of the CFF95 force field[65−67] find the same array of important minima on the (1→6) energy surface revealed in the present work.[68] Contributions from solvation were estimated in these latest calculations using the Poisson−Boltzmann solvation software available as a part of the Jaguar quantum chemistry package.[69,70]

The relative energies of minima A_6−F_6 as determined here and by other workers are in only partial agreement. At the present time no force field has been introduced for carbohydrates that is demonstrated to be generally transferable among different molecules and consistent with a wide range of experimental data, including data on dissolved species.[71] We are therefore satisfied to have attained only general agreement with previous results for the isomaltose conformational energy surface. Our approach has been to use AMBER* with the GB/SA solvation treatment to provide a first approximation to the characteristics of the potential of mean force for the pullulan backbone segments in $\phi,\psi,(\omega)$ space. This has provided an initial set of rotational isomeric states with corresponding statistical weights that reflect not only the energies at the minima on the surface but also the general breadth and depth of the minima. From this starting point we have felt free to make small adjustments to the relative weights of the RIS states to obtain the best possible fit to the solution data at hand. We emphasize that the relative weights we have given to states A_6−F_6 in model 4 are wholly within the range generated by other approaches to approximating the potential of mean force for isomaltose.[60,61,68] The RIS states and their relative weights corresponding to model 4 for the (1→6)-linkage stand on their ability to reproduce a sizable array of data for aqueous pullulan and its oligomers. We intend to test this model for its ability to reproduce the dynamical behavior of the chain using the ORZLD approach.[23,25,26]

Conclusions

A rotational isomeric state model of aqueous pullulan has been developed that is consistent with the chain dimensions of pullulan oligomers with DP = 1, 2, 3, and 4 as determined by small-angle X-ray scattering, with the unperturbed dimensions of high molecular weight pullulan determined by light scattering, and with the temperature coefficient of the unperturbed dimensions. Three important rotational isomeric states (A_6, B_6, and C_6, encompassing together more than 77% of the probability distribution) are identified for the (1→6)-linkage while a single state is used to represent the (1→4)-linkage. One of the states for the (1→6)-linkage (C_6) may be stabilized by a hydrogen bond that spans the linkage and introduces a bend into the chain trajectory. We were able to fit the full array of available experimental evidence only when this state for the (1→6)-linkage was accorded significant weight.

Acknowledgment. This work has been supported by NIH Grant GM 33062 to D.A.B., by a grant from Ohkura Pharmaceutical Co. Ltd. to S.K., and by a Grant-in-Aid for Scientific Research on Priority Areas from the Ministry of Education and Culture, Japan, to K.K. The synchrotron SAXS measurements were performed with authorization from the Photon Factory Advisory Committee (Proposal No. 94G293). Alan Davis and Jennifer Humphries provided assistance in the preparation and analysis of the experimental samples. We are indebted to a referee for drawing our attention to the features of the panose fragment.

References and Notes

(1) Colson, P.; Jennings, H. J.; Smith, I. C. P. *J. Am. Chem. Soc.* **1974**, *96*, 6, 8081−8087.
(2) Yalpani, M. *Polysaccharides*; Elsevier: Amsterdam, 1988.
(3) Tsujisaka, Y.; Mitsuhashi, M. Pullulan. In *Industrial Gums: Polysaccharides and Their Derivatives*, 3rd ed.; Whistler, R. L., BeMiller, J. N., Eds.; Academic Press: San Diego, 1993; pp 447−460.
(4) Morris, V. J. In *Food Polysaccharides and Their Applications*; Stephen, A. M., Ed.; Marcel Dekker: New York, 1995; pp 341−375.
(5) Kato, T.; Okamoto, T.; Tokuya, T.; Takahashi, A. *Biopolymers* **1982**, *21*, 1623−1633.
(6) Kato, T.; Katsuki, T.; Takahashi, A. *Macromolecules* **1984**, *17*, 1726−1730.
(7) Kawahara, K.; Ohta, K.; Miyamoto, H.; Nakamura, S. *Carbohydr. Polym.* **1984**, *4*, 335−356.
(8) Buliga, G. S.; Brant, D. A. *Int. J. Biol. Macromol.* **1987**, *9*, 71−76.
(9) Muroga, Y.; Yamada, Y.; Noda, I.; Nagasawa, M. *Macromolecules* **1987**, *20*, 3003−3006.
(10) Nishinari, K.; Kohyama, K.; Williams, P. A.; Phillips, G. O.; Burchard, W.; Ogino, K. *Macromolecules* **1991**, *24*, 5590−5593.
(11) Nordmeier, E. *J. Phys. Chem.* **1993**, *97*, 5770−5785.
(12) Pavlov, G.; Korneeva, E. V.; Yevlampieva, N. P. *Int. J. Biol. Macromol.* **1994**, *16*, 318−323.
(13) Brant, D. A.; Burton, B. A. The Configurational Statistics of Pullulan and Some Related Glucans. In *Solution Properties of Polysaccharides*; Brant, D. A., Ed.; American Chemical Society: Washington, DC,1981; Vol. 150, pp 81−99.
(14) Burton, B. A.; Brant, D. A. *Biopolymers* **1983**, *22*, 1769−1792.
(15) Buliga, G. S.; Brant, D. A. *Int. J. Biol. Macromol.* **1987**, *9*, 77−86.
(16) Benesi, A. J.; Brant, D. A. *Macromolecules* **1985**, *18*, 1109−1116.
(17) Levy, R. M.; Karplus, M.; Wolynes, P. G. *J. Am. Chem. Soc.* **1981**, *103*, 5998−6011.
(18) Lipari, G.; Szabo, A. *J. Am. Chem. Soc.* **1982**, *104*, 4546−4559.
(19) Bovey, F. A.; Jelinski, L. W. *J. Phys. Chem.* **1985**, *89*, 571−583.
(20) Peng, J. W.; Wagner, G. *J. Magn. Reson.* **1992**, *98*, 308−332.
(21) Brant, D. A.; Liu, H.-S.; Zhu, Z. S. *Carbohydr. Res.* **1995**, *278*, 11−26.
(22) Brant, D. A. *Pure Appl. Chem.* **1997**, *69*, 1885−1892.
(23) Perico, A.; Mormino, M.; Urbani, R.; Cesàro, A.; Tylianakis, E.; Dais, P.; Brant, D. A. *J. Phys. Chem. B* **1999**, *103*, 8162−8171.
(24) Kadkhodaei, M.; Wu, H.; Brant, D. A. *Biopolymers* **1991**, *31*, 1581−1592.
(25) Perico, A. *Biopolymers* **1989**, *28*, 1527−1540.
(26) Perico, A. *Acc. Chem. Res.* **1989**, *22*, 336−342.
(27) Hu, Y.; MacInnis, J. M.; Cherayil, B. J.; Fleming, G. R.; Freed, K. F.; Perico, A. *J. Chem. Phys.* **1990**, *93*, 822−836.
(28) Hu, Y.; Fleming, G. R.; Freed, K. F.; Perico, A. *Chem. Phys.* **1991**, *158*, 395−408.
(29) Mimura, M.; Kitamura, S.; Gotoh, S.; Takeo, K.; Urakawa, H.; Kajiwara, K. *Carbohydr. Res.* **1996**, *289*, 25−37.

(30) Kitamura, S.; Minami, T.; Nakamura, Y.; Isuda, H.; Kobayashi, H.; Mimura, M.; Urakawa, H.; Kajiwara, K.; Ohno, S. *J. Mol. Struct. (THEOCHEM)* **1997**, 425−435.
(31) Kitamura, S.; Isuda, H.; Shimada, J.; Takada, T.; Takaha, T.; Okada, S.; Mimura, M.; Kajiwara, K. *Carbohydr. Res.* **1997**, *304*, 303−314.
(32) Koizumi, K.; Kubota, Y.; Tanimoto, T.; Okada, Y. *J. Chromatogr.* **1989**, *464*, 365−373.
(33) Elias, H.-G. *Macromolecules*; Plenum Press: New York, 1977; Vol. 1.
(34) Kajiwara, K.; Hiragi, Y. Structure Analysis by Small-Agle X-ray Scattering. In *Applications of Synchrotron Radiation to Materials Analysis*; Saisho, H., Gohshi, Y., Eds.; Elsevier: New York, 1996; pp 353−404.
(35) Mohamadi, F.; Richards, N. G. J.; Guida, W. C.; Liskamp, R.; Lipton, M.; Caulfield, C.; Chang, G.; Hendrickson, T.; Still, W. C. *J. Comput. Chem.* **1990**, *11*, 440−467.
(36) Qiu, D.; Shenkin, P. S.; Hollonger, F. P.; Still, W. C. *J. Phys. Chem. A* **1997**, *101*, 3005−3014.
(37) Still, W. C.; Tempczyk, A.; Hawley, R. C.; Hendrickson, T. *J. Am. Chem. Soc.* **1990**, *112*, 6127−6129.
(38) Pérez, S.; Marchessault, R. H. *Biopolymers* **1979**, *18*, 2369−2374.
(39) Nishida, Y.; Hori, H.; Ohrui, H.; Meguro, H. *J. Carbohydr. Chem.* **1988**, *7*, 239−250.
(40) Bock, K.; Duus, J. O. *J. Carbohydr. Chem.* **1994**, *13*, 513−543.
(41) Wolfe, S. *Acc. Chem. Res.* **1972**, *5*, 102−111.
(42) Ferrier, R. J.; Collins, P. M. *Monosaccharides: Their Chemistry and Their Roles in Natural Products*; John Wiley & Sons: New York, 1995.
(43) Kirby, A. J. *Stereoelectronic Effects*; Oxford University Press: New York, 1996.
(44) Senderowitz, H.; Parish, C.; Still, W. C. *J. Am. Chem. Soc.* **1996**, *118*, 2078−2086.
(45) Senderowitz, H.; Still, W. C. *J. Phys. Chem. B* **1997**, *101*, 1409−1412.
(46) Senderowitz, H.; Still, W. C. *J. Org. Chem.* **1997**, *62*, 1427−1438.
(47) Brant, D. A.; Goebel, K. D. *Macromolecules* **1975**, *8*, 522−530.
(48) Brant, D. A. *Q. Rev. Biophys.* **1976**, *9*, 527−596.
(49) Brant, D. A.; Christ, M. D. Realistic Conformational Modeling of Carbohydrates. In *Computer Modeling of Carbohydrate Molecules*; French, A. D., Brady, J. W., Eds.; American Chemical Society: Washington, DC, 1990; Vol. 430, pp 42−68.
(50) Kitamura, S.; Okamoto, T.; Nakata, Y.; Hayashi, T.; Kuge, T. *Biopolymers* **1987**, *26*, 537−548.
(51) Flory, P. J. *Principles of Polymer Chemistry*; Cornell University Press: Ithaca, NY, 1953.
(52) Flory, P. J. *Statistical Mechanics of Chain Molecules*; Wiley-Interscience: New York, 1969.
(53) Mattice, W. L.; Suter, U. W. *Conformational Theory of Large Molecules*; John Wiley & Sons: New York, 1994.
(54) *Small-Angle X-ray Scattering*; Glatter, O., Kratky, O., Eds.; Academic Press: London, 1982; p 515.
(55) *Mathematical, Physical and Chemical Tables*; Wilson, A. J. C., Ed.; The International Union of Crystallography, Kluwer Academic Publishers: Boston, 1992; Vol. C.
(56) Guinier, A. *X-Ray Diffraction in Crystals, Imperfect Crystals, and Amorphous Bodies*; W. H. Freeman and Company: San Francisco, 1963.
(57) Jordan, R. C.; Brant, D. A.; Cesàro, A. *Biopolymers* **1978**, *17*, 2617−2632.
(58) Burchard, W. Theory of Cyclic Macromolecules. In *Cyclic Polymers*; Semlyen, J. A., Ed.; Elsevier Applied Science Publishers: New York, 1986; pp 43−84.
(59) Jeffrey, G. A.; Huang, D.-B. *Carbohydr. Res.* **1991**, *222*, 47−55.
(60) Dowd, M. K.; Reilly, P. J.; French, A. D. *Biopolymers* **1994**, *34*, 625−638.
(61) Tvaroska, I.; Imberty, A.; Pérez, S. *Biopolymers* **1990**, *30*, 369−379.
(62) Lemieux, R. U. Rearrangements and Isomerizations in Carbohydrate Chemistry. In *Molecular Rearrangements, Part 2*; de Mayo, P., Ed.; John Wiley & Sons: New York, 1964; pp 7009−7069.
(63) Cramer, C. J.; Truhlar, D. G.; French, A. D. *Carbohydr. Res.* **1997**, *298*, 1−14.
(64) Cerius^2, 3.5 ed.; Molecular Simulations, Inc.: San Diego, CA, 1997.
(65) Maple, J. R.; Dinur, U.; Hagler, A. T. *Proc. Natl. Acad. Sci. U.S.A.* **1988**, *85*, 5350−5354.
(66) Dinur, U.; Hagler, A. T. *J. Comput. Chem.* **1990**, *11*, 1234−1246.
(67) Maple, J. R.; Hwang, M. J.; Stockfisch, T. P.; Dinur, U.; Waldman, M.; Ewig, C. S.; Hagler, A. T. *J. Comput. Chem.* **1994**, *15*, 162−182.
(68) Liu, J. H.-Y.; Brameld, K. A.; Brant, D. A.; Goddard III, W. A., submitted for publication.
(69) Ringnalda, M. N.; Langlois, J.-M.; Greeley, B. H.; Murphy, R. B.; Russo, T. V.; Cortis, C.; Muller, R. P.; Marten, B.; Donnelly, R. E.; Mainz, D. T.; Wright, J. R.; Pollard, W. T.; Cao, Y.; Won, Y.; Miller, G. H.; Goddard, W. A. III.; Friesner, R. A. Jaguar 3.0; Schrödinger, Inc.: Portland, OR, 1997.
(70) Mainz, D. PBF Script, personal communication.
(71) Jónsdóttir, S. Ó.; Welsh, W. J.; Rasmussen, K.; Klein, R. A. *New J. Chem.* **1999**, *23*, 153−163.

MA990591H